BULLETIN OF THE POLISH ACADEMY OF SCIENCES
TECHNICAL SCIENCES
Vol. 52, No. 3, 2004

High altitude long endurance unmanned aerial vehicle of a new generation – a design challenge for a low cost, reliable and high performance aircraft

Z. GORAJ[1]*, A. FRYDRYCHEWICZ[1], R. ŚWITKIEWICZ[1], B. HERNIK[1], J. GADOMSKI[1], T. GOETZENDORF-GRABOWSKI[1], M. FIGAT[1], St. SUCHODOLSKI[1] and W. CHAJEC[2]

[1] Institute of Aeronautics and Applied Mechanics, Warsaw University of Technology, 24 Nowowiejska St., 00–665 Warszawa, Poland
[2] PZL Mielec, 3 Wojska Polskiego St., 39–300 Mielec, Poland

Abstract. This paper describes a design process of HALE PW-114 sensor-craft, developed for high altitude (20 km) long endurance (40 h) surveillance missions. Designed as a blended wing (BW) configuration, to be made of metal and composite materials. Wing control surfaces provide longitudinal balance. Fin in the rear fuselage section together with wingtips provide directional stability. Airplane is equipped with retractable landing gear with controlled front leg that allows operations from conventional airfields. According to the initial requirements it is twin engine configuration, typical payload consists of electro-optical/infra-red FLIR, big SAR (synthetic aperture radar) and SATCOM antenna required for the longest range. Tailless architecture was based on both Horten and Northrop design experience. Global Hawk was considered as a reference point – it was assumed that BW design has to possess efficiency, relative payload and other characteristics at least the same or even better than that of Global Hawk. FLIR, SAR and SATCOM containers were optimised for best visibility. All payload systems are put into separate modular containers of easy access and quickly to exchange, so this architecture can be consider as a „modular". An optimisation process started immediately when the so-called "zero configuration", called PW-111 was ready. It was designed in the canard configuration. A canard was abandoned in HALE PW-113. Instead, new, larger outer wing was designed with smaller taper ratio. New configuration analysis revealed satisfactory longitudinal stability. Calculations suggested better lateral qualities for negative dihedral. These modifications, leading to aerodynamic improvement, gave HALE PW-114 as a result.

The design process was an interdisciplinary approach, and included a selection of thick laminar wing section, aerodynamic optimisation of swept wing, stability analysis, weight balance, structural and flutter analysis, many on-board redundant systems, reliability and maintability analysis, safety improvement, cost and performance optimisation. Presented paper focuses mainly on aerodynamics, wing design, longitudinal control and safety issues. This activity is supported by European Union within V FR, in the area Aeronautics and Space.

Keywords: aircraft, UAV, stability, structure, flutter, safety.

Notations

Acronims

BWB	Blended Wing Body
COTS	Commercial Off The Shelve
DLM	Doublet Lattice Method
EO/IR	ElectroOptical InfraRed
FLIR	Forward Looking Infra Red
GCS	Ground Control Station
HALE	High Altitude Long Endurance
LE	Leading Edge
SATCOM	Satellite Communications
MAC	Mean Aerodynamic Chord
MTBCF	Mean Time Between Critical Failures
MTBL	Mean Time Between Losses
MTBUCL	Mean Time Between Uncontrolled Landing
SAR	Synthetic Aperture Radar
SIGINT	Signal Intelligence
TE	Trailing Edge
UAV	Unmanned Aerial Vehicle

Symbols

a, a_1	lift curve slope for main wing and canard, respectively
b	chord length
c_a	value of MAC
c_f	elevon chord
c_r	root chord
c_D	drag coefficient
c_{Di}	induced drag coefficient
C_L	lift coefficient
C_{LC}	lift coefficient on canard
C_{mN}	pitching moment coefficient about neutral point
$C_{mA,W+B}$	pitching moment coefficient about point A (0.25% of MAC), for wing and body
f_B, f_1, f_2, f_3	fuel in body, inner, middle and outer tanks
g	structural damping coefficient
G	shear modulus
k	reduced frequency (Strouhal number)
K	kernel function
l_C	arm of canard with respect to point A
Ma	Mach number
q	dynamic pressure
Q	aircraft weight

* e-mail: goraj@meil.pw.edu.pl

Q(t) critical failures probability (unreliability)
R(t) reliability
Re Reynolds number
S wing gross area
S_c canard gross area
St designation of structure and on-board equipment
U_∞ undisturbed flow velocity
w displacement normal to lifting surface; balance weight placed in the wing tip
x_N distance from point A (0.25% of MAC) to point N (neutral point)
α angle of attack
δ_F elevon deflection (positive if TE goes down)
ϕ_i i-th natural mode
Δh static stability margin (positive if centre of gravity ahead of neutral point)
Δp pressure difference
ξ_i generalized coordinate of the i-th natural mode $\phi_i(x, y)$
ω natural frequency

1. Introduction

Many European and American experts predict that within 10 years UAVs will be operated within Civilian Airspace on behalf of many Civilian and Commercial missions [1–5]. To happen it some regulatory issues have to be set up and further technology development have to be done. The most important directions of these progress-creating activities include:

(1) Increased utilisation and miniaturization of military UAVs;

(2) Technology development, mainly improved reliability, safety and performance;

(3) Reduced manufacturing and operating cost and (4) Increased acceptance by civilian authorities [6–9].

Among the most important UAV's application there are:

(1) Dangerous missions where UAVs are almost only solution. They include poisonous environment; radiation disaster hazard; extreme high altitudes and severe weather conditions;

(2) Scientific mission where UAVs are best solution and economic issue is secondary. They include environmental monitoring; weather forcasting; atmospheric data collection; oceanographic data collection; agricultural hyperspectral imaging and magnetic, radiological, gravimetric mapping;

(3) Commercial missions where UAVs are not sole solution and do have sense if are commercially viable.

They include border surveillance; city automobile traffic monitoring; airborne cellular antenna; wildland monitoring and fire-fighting; pipelines and power line monitoring; poor man's satellite relay.

Under the auspices of European Union the CAPECON project [10] has been launched. This project's goal is to develop a number of UAV platforms being effective in their missions [11, 12], safe, reliable and relatively cheap in application [13, 14]. An essential effort of CAPECON activity is focused on High Altitude Long Endurance platforms (HALE), and among them on Blended Wing Body (BWB) configuration [15]. Such HALEs platforms are often called "sensor-crafts" due to the fact that they are carriers for various sensors (SAR, SIGINT, FLIR, etc), [16–21].

The main requirements for HALE-UAV BW configuration are defined in Tab. 1.

Table 1
Requirements developed for BWB HALE aircraft under CAPECON project [10]

Parameter	Requirement	Extreme value(s)
Altitude	60 000ft on loiter	65 000 ft
Flight speed	Mach 0.6 at loiter alt.	max Mach number: 0.65 due to aerodynamic efficiency (dramatically increase of wave drag on airfoils)
Endurance	24 h on loiter	Min 8 h
Range	1000 km	200-1000 km
Take off & landing	Use of conventional airports	
Payload weight	500 kg	Min 350 kg
Power taping	8 kW	
Climb performance	55 000 ft reached in 30 min	Less than 1 hour
Payload volume or dimensions (Length × width × height)	Sensor equipment area (several racks) : 0.5 m^3	
	SAR antenna : 1.1 m × 0.5 m × 0.3 m	0.4 to 0.6 m^3 - Racks (units) dimensions are typically 0.5 m × 0.5 m × 0.5 m
	EO/IR sense part: 1 m × 0.7 m × 0.7 m	Max SAR antenna: 2.5 m × 0.6 m × 0.5 m
Communication	SATCOM antenna volume: sphere of 1.0 m diameter	The use of SATCOM antenna depends on range

HALE PW-114 was developed for high altitude (20 km) long endurance (40 h) surveillance missions. Designed as a blended wing (BW) configuration, to be made of metal and composite materials. It is equipped with two engines, FJ44-3, optimised for high altitude flights. Wing control surfaces provide longitudinal balance. Fin in the rear fuselage section together with wingtips provide directional stability. Airplane is equipped with retractable landing gear with controlled front leg that allows operations from conventional airfields. According to the initial requirements it is twin engine configuration, typical payload consists of electro-optical/infra-red FLIR, big SAR (synthetic aperture radar) and SATCOM antenna required for the longest range. Tailless architecture was based on both Horten and Northrop design experience. Global Hawk was considered as a reference point [22–24] – it was assumed that BW design has to possess efficiency, relative payload (Payload over the total weight) and other characteristics at least the same or even better than that of Global Hawk. FLIR, SAR and SATCOM containers were optimised for best visibility. No one element of aircraft structure limits the sensor's visibility. All payload systems are put into separate modular containers of easy access and quickly to exchange, so this architecture can be consider as a „modular". An optimisation process started immediately when the so-called "zero configuration", called PW-111 was ready. It was designed in the canard configuration. Vertical stabilizer was located under rear part of the centre-wing. This configuration provided high manoeuvrability. However it had to be redesigned because of too large canard loading and longitudinal instability. HALE PW-112 received modified canard. Moreover fuselage and engine nacelle geometry was modified. Lower front fuselage section had to be enlarged because front leg of landing gear was moved forward to the fuselage nose. Previously, front landing gear leg had been located behind EO/IR sensor. Nacelles had to be enlarged after final engine selection.

The canard was abandoned in HALE PW-113. Instead, new, larger outer wing was designed with smaller taper ratio. A new configuration analysis revealed satisfactory longitudinal stability. Unfortunately lateral stability appeared not to be satisfactory. The vertical stabilizer with rudder was located at the top of the fuselage. Calculations suggested better qualities for negative dihedral. These modifications of PW-113, leading to aerodynamic improvement, gave HALE PW-114 as a result [15].

The design process was an interdisciplinary approach, and included a selection of thick laminar wing section, aerodynamic optimisation of swept wing, stability analysis, weight balance, structural and flutter analysis, many on-board redundant systems, reliability and maintability analysis, safety improvement, cost and performance optimisation. This activity was supported by European Union within V FR, in the area Aeronautics and Space.

2. Global Hawk as a baseline aircraft

There is a huge diversity in the configuration layouts, power units, take-off and landing systems, avionic systems etc. which may be seen in flying unmanned vehicles (micro UAVs, small-close-range UAVs, MALE UAVs and HALE UAVs). In many cases it is easy to see why a particular design solution has been chosen (for example a two-beam fuselage arrangement in many MALE configurations), but sometimes it is not easy to explain for example, why the dihedral angle of a MALE V-tailplane is negative instead of positive. A specific geometrical solution should be appropriate to the prescribed mission, including payload, antennas, avionics, radars, sensors and instrumentation etc. As a result very strange shapes are often observed, for example X–45, Global Hawk [25], Dark Star etc. It seems that often the final shape is a matter of trade-off between aerodynamic efficiency, the flight control system (usually very expensive), stealth (in the military sector), payload, reliability and safety. The design layout for both manned and unmanned aerial vehicles depends on type of the mission, speed, requirements following from on-board payload, power unit and its integration with the structure, chief designer predilection and sometimes the current fashion. In some cases the same mission can be effectively fulfilled by different layouts, especially if the mission is not very "demanding" and difficult with respect to performance, reliability and safety issues. However, for extreme missions (for example long endurance, high altitude flights with payloads requiring a very wide area of observation unshielded by engines and other on-board equipment) the constraints are usually very demanding. For example, if SATCOM (see Fig.1) and SAR are located in the forward fuselage section the power unit must be placed in the rear fuselage. Flexible missions (i.e. missions of requiring varying endurances, different types and weights of payload) can be more easily accomplished using compact, double-beam fuselage configurations which are usually less sensitive to the change of weight. Many Israeli UAVs (Searcher, Heron, Hunter etc.) have such a double-beam layout. A pushing propeller in such configurations is a natural choice, not limiting the seeing capabilities of the front-body sensors. Long fuselage arrangement (with the Predator as a typical representative of this layout) is very effective for surveillance missions with the same kind of payload. However, any change in the weight of payload in the front part of fuselage changes the location of the centre of gravity and should be compensated by replacement of fuel, elevator deflection etc.

The high aspect ratio wing of Global Hawk (Fig. 2) is essential to reduce the induced drag, especially at the beginning of the mission, when the lift coefficient is of the order of unity. Selected performance parameters were computed [13,16] basing on overall dimensions and weights gleaned from published material including for example technical journals, manufacturers' publications and appropriate web sites. An example of performance param-

eters for both Global Hawk and Predator are presented in Fig. 3.

All three layouts (Fig. 4) are different. Global Hawk is powered by a turbofan engine, has the highest aspect ratio wing with a slightly swept leading edge. It operates at high altitude with Mach number of 0.60. Predator is powered by a Rotax piston engine, has a straight wing and is designed for one type of mission. Any changes in payload, located at nose of the fuselage, can essentially change the weight distribution.

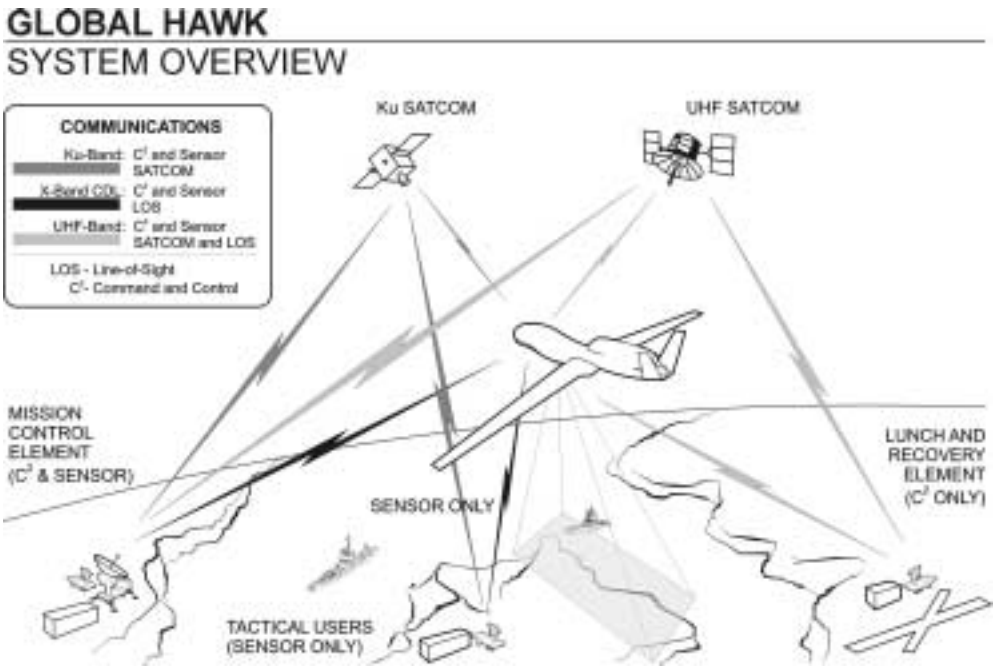

Fig. 1. Communication system overview: Ku, X and UHF bands (after Ref. 13)

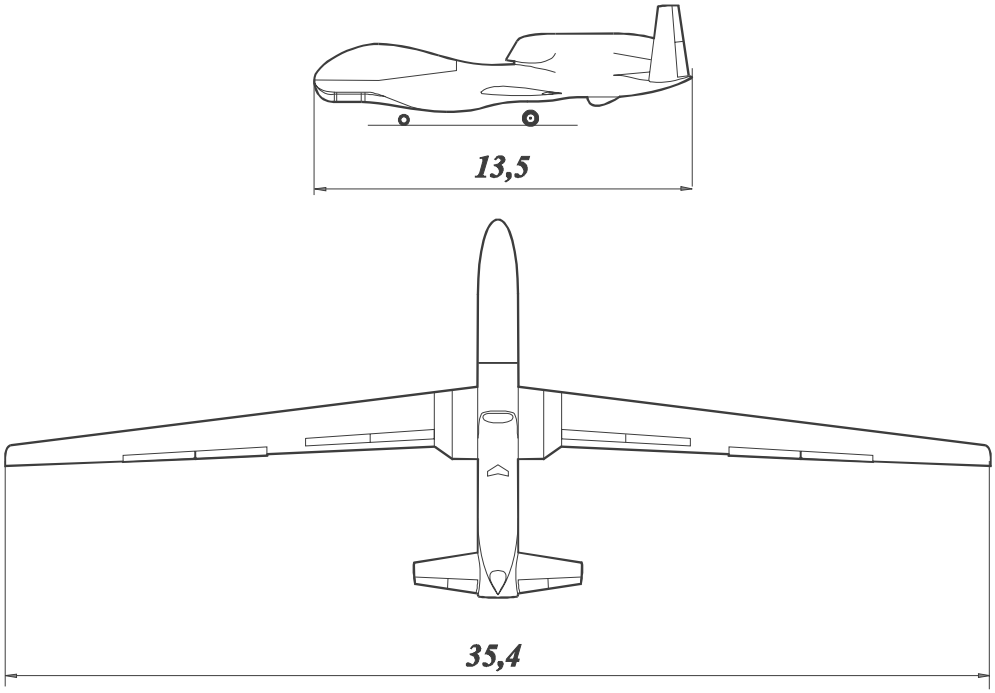

Fig. 2. GLOBAL HAWK – general arrangement (configuration based on Web-site sources, after Ref. 25)

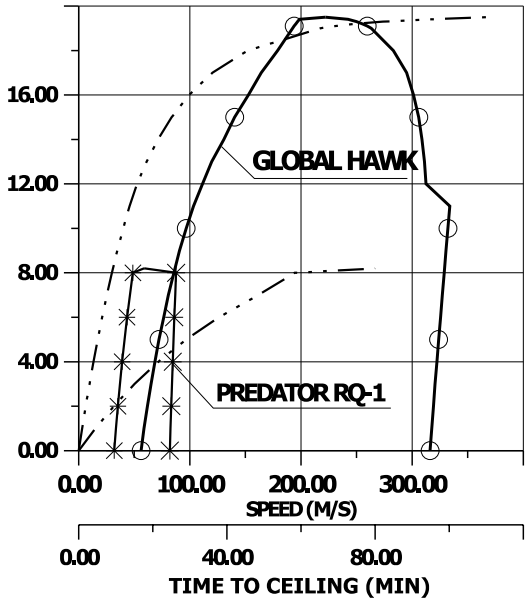

Fig. 3. Global Hawk and Predator – flight envelopes (after Ref. 16)

Global Hawk was used in the CAPECON HALE BWB design process as a baseline aircraft. From the same beginning of design effort it was assumed that one must create an aircraft being comparable to Global Hawk in terms of performance, cost and safety. Otherwise, the whole project would not have any sense and no customer in the future. Some important geometrical, weight and other Global Hawk characteristics are shown in Tables 2 and 3.

Table 2
Global Hawk – selected geometrical and weight parameters (after Refs. 16, 25)

Wing span	35.42 m
Length	13.52 m
Height	4.60 m
Wing area	50.2 m^2
Aspect ratio	25.09
Equipped empty weight	4177 kg
Take-off weight	11622 kg
Fuel weight	6583 kg
Mission equipment weight	900 ÷ 1000 kg

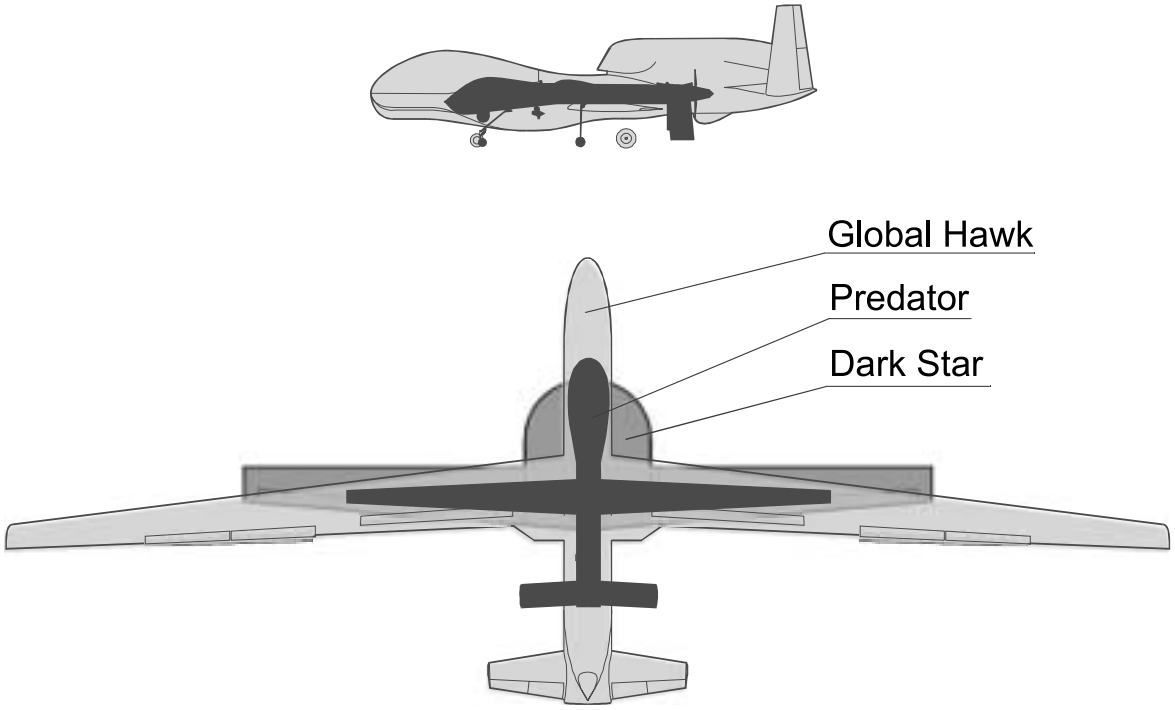

Fig. 4. Comparison of the three Tier projects' layouts: Global Hawk (Tier II+) after Ref. 25, Predator QR (Tier II)[26] and DarkStar (Tier III-),

(after Refs. 16, 25 and 26)

Table 3
Global Hawk – selected performances (after Refs. 16, 25)

Stall speed	170 km/h
Loiter speed	650 km/h
Max speed	670 km/h
Ceiling	19.80 km
Rate of climb	17.3 m/s
endurance	38 ÷ 42 h
range	17 000 km
Runway length	1500 m
Take-off thrust	3.13 kN
Wing loading	231.52 kg/m^2
Thrust loading	37.1 kg/N

3. Design process

3.1. Preliminary layout: PW-111. PW-111 UAV was designed as a canard configuration. Vertical stabilizer was located under rear part of the centre-wing. This configuration provided high manoeuvrability. However, following the results of static and dynamic computation it appeared that this design had to be optimised because of too large canard loading and longitudinal instability.

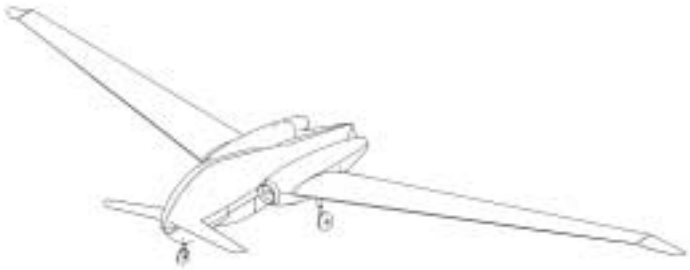

Fig. 5. HALE PW-111

3.2. Optimised canard: PW-112. HALE PW-112 received a modified, higher aspect ratio canard. Moreover fuselage and engine nacelle geometry was modified. Lower front fuselage section had to be enlarged because front leg of landing gear was moved forward to the fuselage nose. Previously, front landing gear leg had been located behind the EO/IR sensor. Nacelles had to be enlarged after the final engine selection. However, loading on the canard was still too large and it become clear that optimisation process did not solve the main drawback of PW-111, i.e. its equilibrium and stability problems. To investigate this problem and then to optimise further the PW-112 layout, i.e. to design a canard the best suited for the main wing, the equations of longitudinal equilibrium have been written. Pitching moment coefficient (only its aerodynamic components) about an unknown neutral point N has the

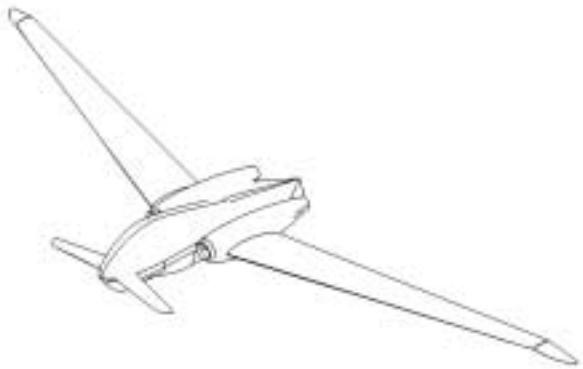

Fig. 6. HALE PW-112 – a general view

form:

$$C_{mN} = C_{mA,W+B} + \frac{C_L x_N}{c_a} + \frac{S_c}{S} C_{LC} \frac{l_C + x_N}{c_a}. \quad (1)$$

Differentiating with respect to lift coefficient and accounting that this pitching moment coefficient is taken about the neutral point one has obtain

$$\frac{\partial C_{mN}}{\partial C_L} = \frac{\partial C_{mA,W+B}}{\partial C_L} + \frac{x_N}{c_a} + \frac{S_c}{S} \frac{\partial C_{LC}}{\partial C_L} \frac{l_H + x_N}{c_a} = 0, \quad (2)$$

where

$$C_{LC} = a_1 \alpha; \frac{\partial C_{LC}}{\partial C_L} = \frac{\partial C_{LC}}{\partial C\alpha} \frac{\partial \alpha}{\partial C_L} = \frac{a_1}{a}. \quad (3)$$

After rewriting one has

$$\frac{\partial C_{mA,W+B}}{\partial C_L} + \frac{x_N}{c_a} + \frac{S_c}{S} \frac{l_C}{c_a} \frac{a_1}{a} + \frac{S_c}{S} \frac{x_N}{c_a} \frac{a_1}{a} = 0; \quad (4)$$

and finally

$$\frac{x_N}{c_a} = \left(-\frac{\partial C_{mA,W+B}}{\partial C_L} - \kappa_C \frac{a_1}{a} \right) \frac{1}{1 + \frac{S_c}{S} \frac{a_1}{a}}. \quad (5)$$

Pitching moment coefficient about the neutral point N (including its mass component) has the form

$$C_{mN} = C_{mA,W+B} + \frac{C_L X_N}{c_a} + \frac{S_c}{S} C_{LC} \frac{l_C + x_N}{c_a} - \frac{Q \Delta h}{q S c_a}, \quad (6)$$

where Δh for naturally stable aircraft should be at least equal to 5% c_a.

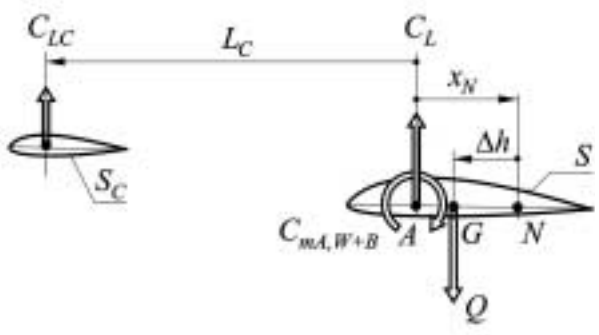

Fig. 7. Characteristic points, forces, moments and dimensions used in mathematical description

Equations (5), (6) can be jointly written in matrix form as follows

$$\mathbf{AX} = \mathbf{B}, \tag{7}$$

where

$$\mathbf{A} = \begin{bmatrix} \frac{1}{c_a} & \frac{a_1}{a} \\ \frac{C_L + \frac{S_c}{S} C_{LC}}{c_a} & C_{LC} \end{bmatrix}; \quad \mathbf{B} = \begin{bmatrix} -\frac{\partial C_{mA,W+B}}{\partial C_L} \\ \frac{Q\Delta h}{qSc_a} - C_{mA,W+B} \end{bmatrix};$$

$$\mathbf{X} = \begin{bmatrix} x_N \\ \kappa_C \end{bmatrix}. \tag{8}$$

Equation (8) has the following solution

$$x_N = \frac{\det \begin{vmatrix} -\frac{\partial C_{mA,W+B}}{\partial C_L} & \frac{a_1}{a} \\ \frac{Q\Delta h}{qSc_a} - C_{mA,W+B} & C_{LC} \end{vmatrix}}{\det(\mathbf{A})};$$

$$\kappa_C = \frac{\det \begin{vmatrix} \frac{1}{c_a} & -\frac{\partial C_{mA,W+B}}{\partial C_L} \\ C_L + \frac{S_c}{S} C_{LC} & \frac{Q\Delta h}{qSc_a} - C_{mA,W+B} \end{vmatrix}}{\det(\mathbf{A})}, \tag{9}$$

whilst

$$\det(\mathbf{A}) = \frac{\mathrm{C_{LC}}}{\mathrm{c_a}} - \frac{C_L + \frac{S_c}{S} C_{LC}}{c_a} \frac{a_1}{a}. \tag{10}$$

Figue 8 shows that independently on the canard area S_C and its lift curve-slope a_C the natural longitudinal stability can be attained when the dimensionless arm $\mathrm{L}_H/\mathrm{c}_a$ is negative, i.e. when the canard is replaced with a classical tailplane.

3.3. Blended Body Wing: PW-113. The canard was abandoned in PW-113 aircraft. Instead, new, larger outer wing was designed with smaller taper ratio. This way the aircraft layout has evolved into a flying wing or the so-called Blended Body Wing configuration. Analysis of this new configuration revealed satisfactory longitudinal stability. Unfortunately transverse stability appeared not to be satisfactory enough. Vertical stabilizer with rudder was located at the top of the fuselage. Calculations suggested better qualities for negative dihedral.

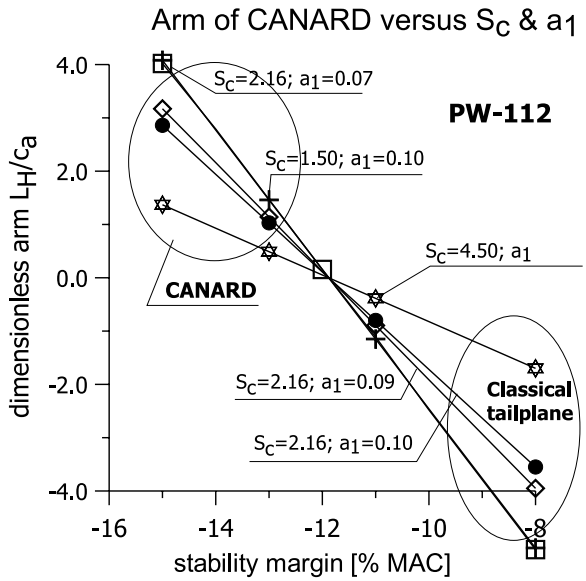

Fig. 8. Effect of canard parameters on HALE PW-111 longitudinal stability

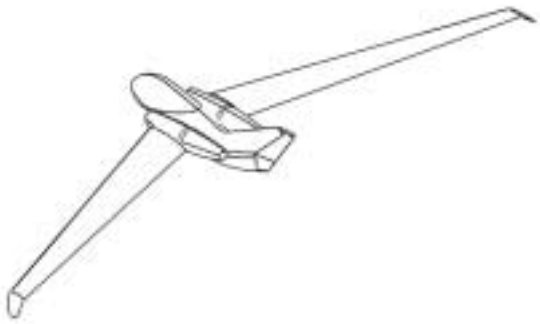

Fig. 9. HALE PW-113 – a general view

The abovementioned modifications leading to the aerodynamic improvement gave PW-114 HALE UAV as a result.

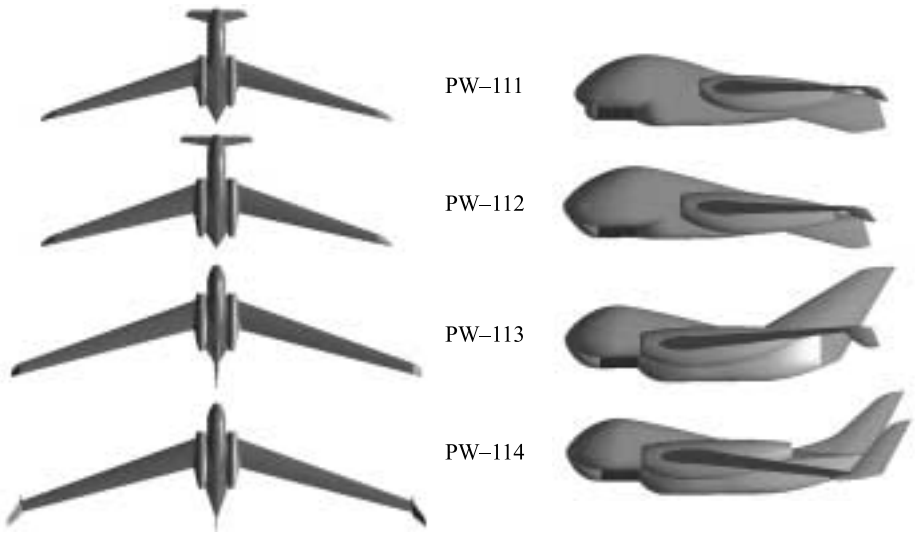

Fig. 10. Comparison of the configurations (top and side views): HALE PW-111, PW-112, PW-113 and PW-114

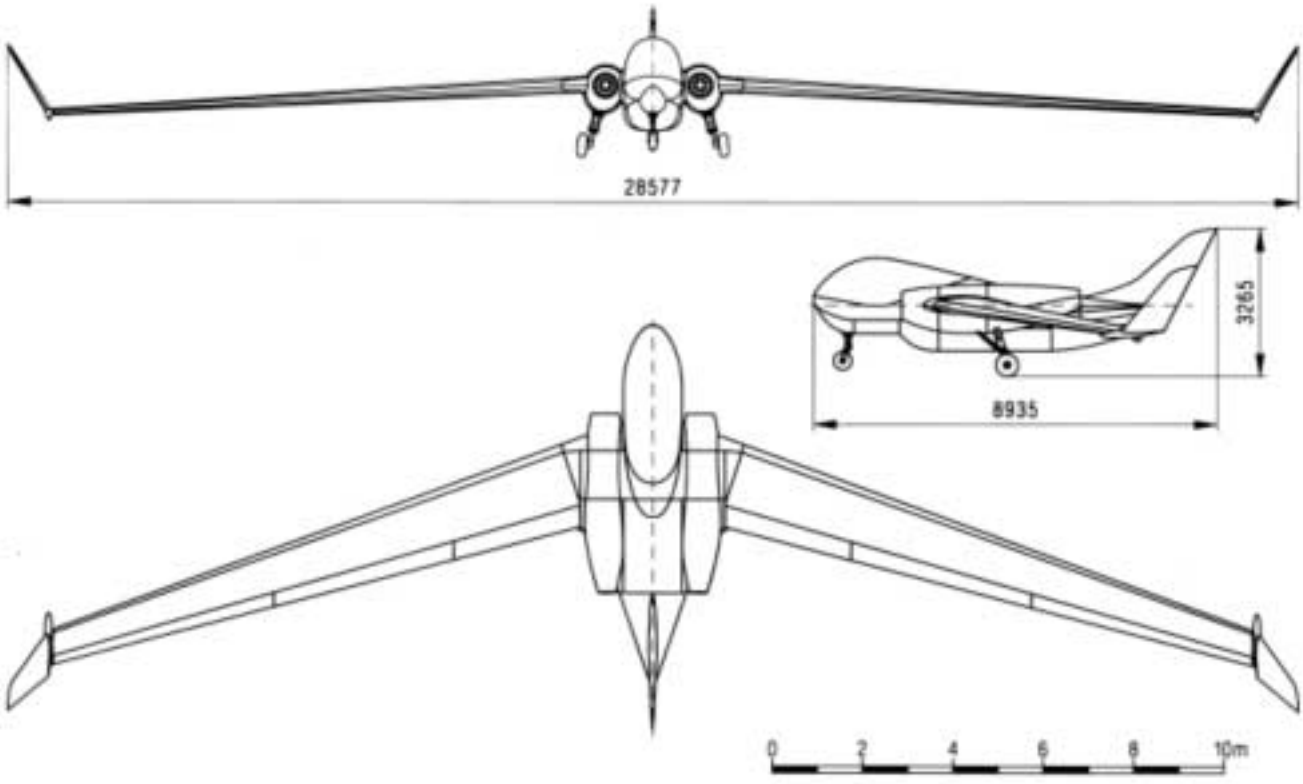

Fig. 11. HALE PW-114 (three views)

3.4. Final layout: PW–114 and its short description. HALE PW-114 is designed as a blended wing configuration, made of metal and composite materials. It is equipped with two engines. Wing control surfaces provide longitudinal balance. Fin in the rear fuselage section together with wingtips provide directional stability. Airplane is equipped with retractable landing gear with controlled front leg that allows operations from conventional airfields.

Table 4
Technical data (after Refs. 10, 15)

Wing span	28 m
Wing area	44.4 m^2
Aspect ratio	17.7
Empty mass	2200 kg
Payload	700 kg
Fuel mass	4150 kg
Take-off mass	6350 kg
Take-off thrust	20.9 kN
Wing loading	143 kg/m^2
Thrust loading	304.1 kg/kN
Payload loading	15.8 kg/m^2
Payload/take-off thrust	33.5 kg/kN

Table 5
HALE PW-114 main geometric data

Reference wing area	44.38 m^2
Span	28 m
Aspect ratio	17.7
MAC (Mean Aerodynamic Chord)	2.02 m
Wing taper ratio	0.355
Wing average thickness t/c	17.5%
Fuselage length	6.95 m
Wetted area breakdown:	
Wing	75.57 m^2
Body	22.82 m^2
Nacelle	13.68 m^2
Vertical stabilizer	7.81 m^2
Total	119.88 m^2
Wing airfoil definition	LRT-17.5
Tail airfoil definition	NACA 0015

4. Aerodynamic analysis

During design process aircraft has been changing. Some parts was improved, some was rejected because are useless in the new configuration. This chapter describes changes in aerodynamic configuration of HALE aircraft from version PW-111 to PW-114. Main parts of aircraft was presented separately to emphasize differences and improvement.

Aerodynamic calculations were made using the VSAERO program. The program uses the potential compressible flow model (subsonic) with boundary layer.

Computation was solved for cruise flight condition:

– Mach number Ma=0.6;
– Reynolds number Re=1E6
– altitude flight (service ceiling) H=19000[m];

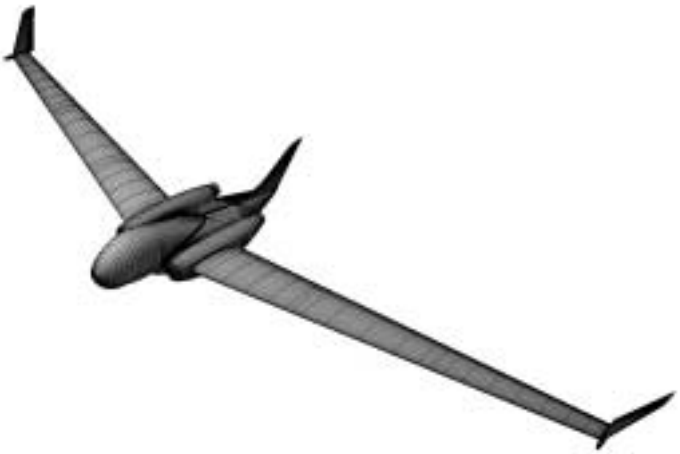

Fig. 12. PW-114 HALE aircraft – 9643 panels

4.1. Wing section. LRT-17.5 wing section was selected, mainly due to its high CL (CL,MAX = 1.54 at Mach=0.57 and CL,MAX = 1.46 at Mach = 0.62 and Re=2*106), needed at loiter regime with Ma=0.6. It us enabled to essentially limit the gross wing area. All aerodynamic characteristics were computed using MSES code (2D + boundary layer), developed by M.Drela. Selected results both for LRT-17.5 and Global Hawk wing section (Fig.13) were compared with that of experimentally investigated by Israel Aircraft Industry [27] and are presented in Fig. 14–16.

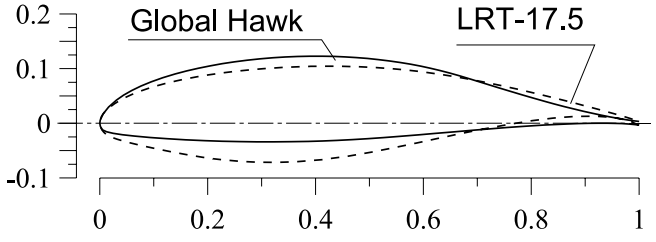

Fig. 13. Airfoil of PW-114 wing compared to the Global Hawk airfoil

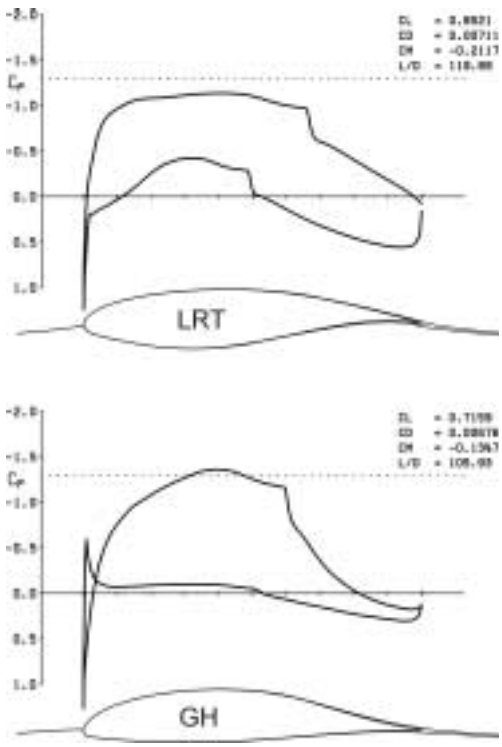

Fig. 14. Cp distribution over LRT 175 wing section and Global Hawk airfoil, from MSES code

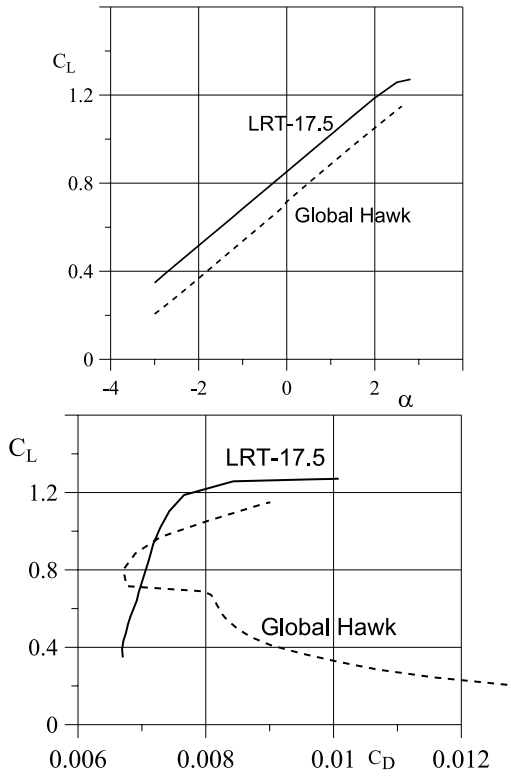

Fig. 15. Lift curve and polar drag for LRT 175 (after Ref. 27) and Global Hawk airfoils computed by MSES code

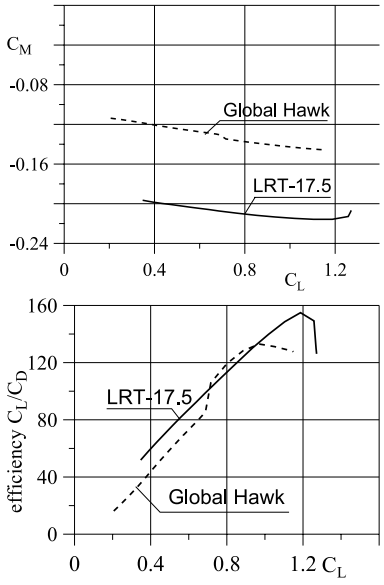

Fig. 16. Pitching moment and aerodynamic efficiency versus lift coefficient for LRT 175 and Global Hawk airfoils computed by MSES code

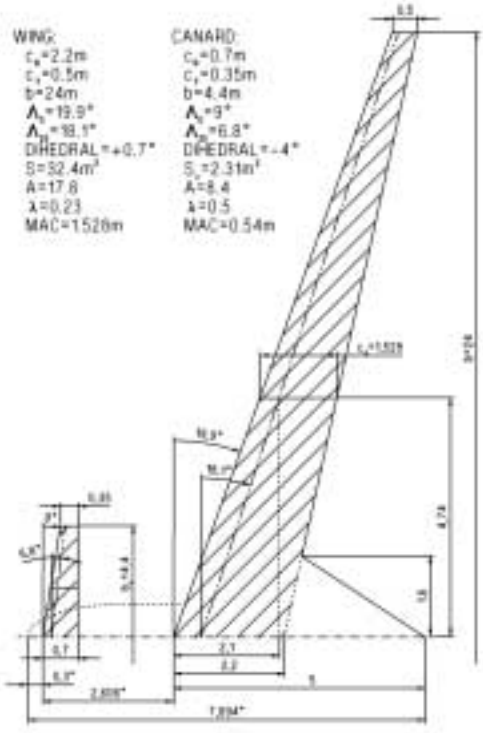

Fig. 17. Wing planform and canard geometry of PW-111 aircraft

4.2. Wing. The first conception of HALE wing assumed medium wing swept angle – 18,6 [deg] of 25% chord line, span dimension equal 24 [m] and small positive dihedral angle. This angle for swept wing gave rather unstable solution but to assure lateral stability, tip of the wing had large negative dihedral angle which compensated positive angle of main wing. This solution had another good feature. Main wing was pushed away from the ground which protected its from damage during take-off or landing phase and provided natural flow of fuel from tip of the wing toward center plane of aircraft.

Fig. 18. PW-113 HALE aircraft – vertical-tail, 3D view

Finally to provide the best lateral stability two vertical surfaces were added. Both of them were placed on tips of the wing. This idea allowed to decrease surface of main stabilizer and the efficiency of this group was increased because two of them are on a big arm and they provided a huge stabilizing moment. Tail-vertical airfoil definition is NACA 64_1-012.

Fig. 20. PW-114 HALE aircraft – vertical stabilizers, 3D view

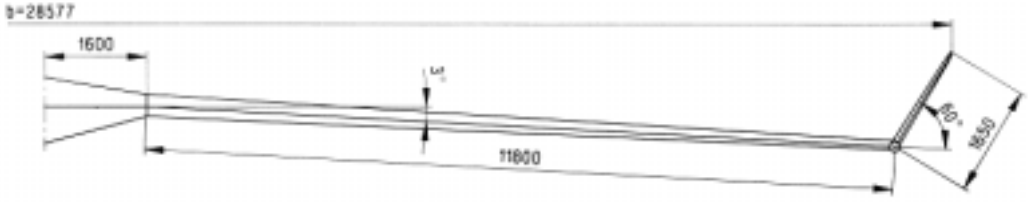

Fig. 19. PW-114 HALE aircraft – geometry of wing stabilizer (front view)

4.3. Fuselage. The main aim of the fuselage of HALE aircraft is to contain all mission equipment. In the preliminary assumption of configuration of HALE aircraft the canard was built in the front of the fuselage. It was the reason why fuselage of PW-111 was longed.

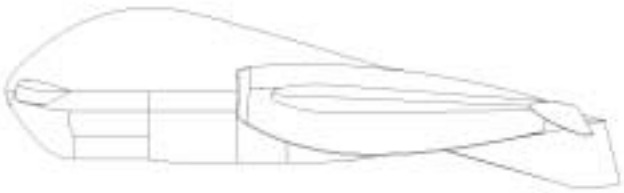

Fig. 21. PW-111 HALE fuselage – side view

Main modification of HALE fuselage was executed, when the canard was rejected. Length of HALE fuselage was decreased, because there was no need to have a long fuselage. Figure below compares a contour of PW-111 and PW-114, main differences are clearly visible.

Fig. 22. Improvement of HALE fuselage of PW-113

After this modification the fuselage of HALE PW-114 was not altered significantly. Only the end of the fuselage was changed. Modification of main vertical stabilizer was the reason to change geometry of HALE fuselage. Final shape and geometry of HALE fuselage was presented in figures below.

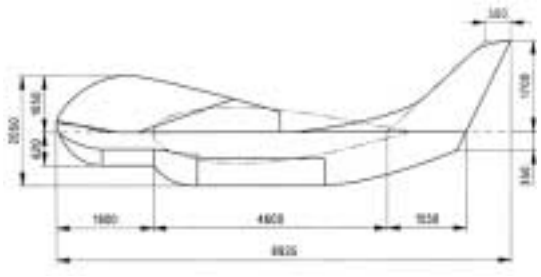

Fig. 23. Fuselage of PW-114 HALE aircraft – side view

Fig. 24. Fuselage of PW-114 HALE aircraft – top view

4.4. Aerodynamic characteristic of whole aircraft. The aircraft surface was divided into a number of small panels, each panel was assumed to have constant pressure distribution. The average number of panels (depending on configuration and a specific version) was about 9 000. The resulting pressure distributions (selected examples) are shown in Fig. 25–27 and correspond to flow around

Fig. 25. Cp distribution for PW-111 HALE aircraft at $\alpha = 0^{\circ}$

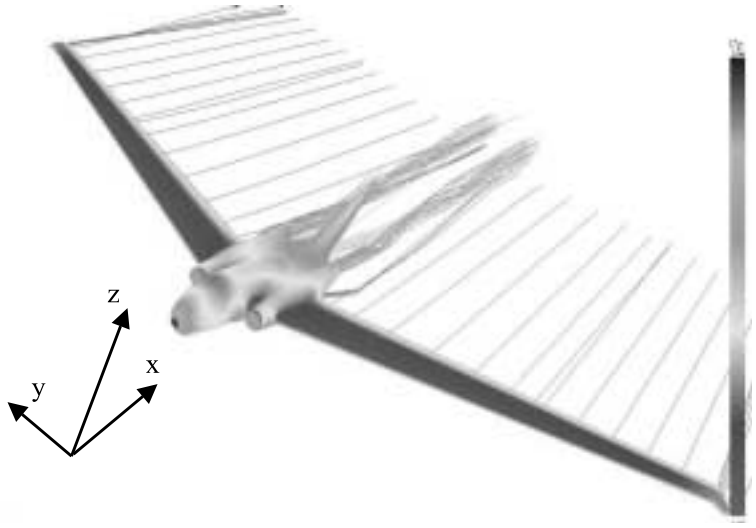

Fig. 26. Cp distribution for PW-113 HALE aircraft at $\alpha = 2^{\circ}$

Fig. 27. Cp distribution for PW -114 HALE aircraft at $\alpha = 1^{\circ}$

the canard configuration (PW-111) at angle of attack equal to zero, the Blended Wing Body configuration with positive dihedral and a single vertical stabilizer located in the rear part of the body (PW-113) at angle of attack equal to 2°, and the Blended Wing Body configuration with negative dihedral and a triplet vertical stabilizer located in the rear part of the body and both wings tips (PW-114) at angle of attack equal to 1°, respectively.

One of the most important tasks to be solved was finding the lift and pitching moments gradients versus control surfaces deflections. These characteristics are typically non-linear and were obtained by successive computations for a number of the control surface's deflections. Some examples of such computations are presented in Figs. 28–29. Gradients of lift and pitching moment for main flaps, aerodynamic brakes and flaperons are shown in Tab. 6.

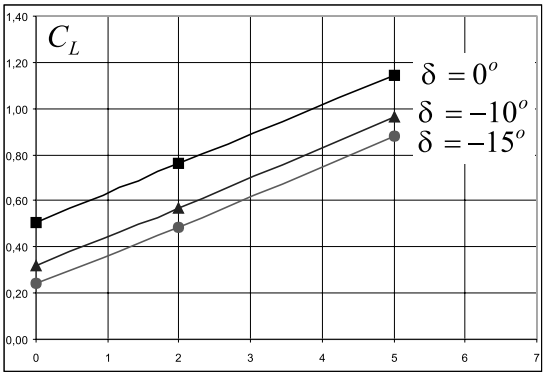

Fig. 28. Lift coefficient $C_L(\alpha, \delta_E)$; $\mathrm{Re} = 2.5 \cdot 10^6$; $Ma = 0.6$

Table 6
Characteristics of control surfaces

Gradients of lift and pitching moment versus flap deflection	$dC_L/d\delta F$	$dC_m/d\delta F$
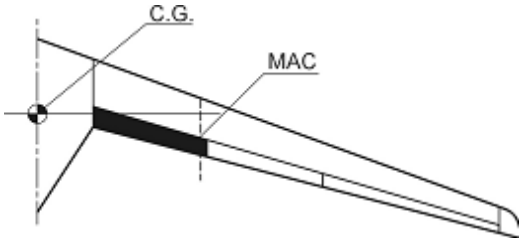	0.0116	0.0024 flap deflected down gives $\Delta C_M > 0$
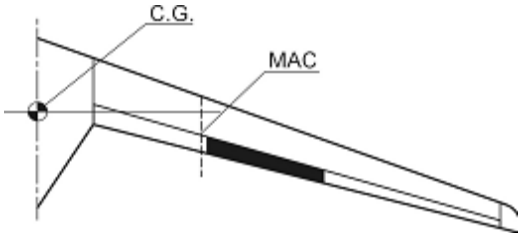	0.0116	-0.0041 flap deflected down gives $\Delta C_M > 0$
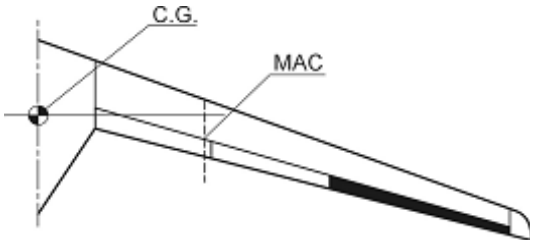	0.020	-0.0163 flap deflected up gives $\Delta C_M > 0$

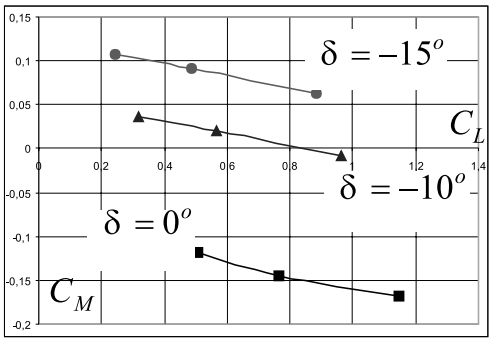

Fig. 29. Pitching moment coefficient $C_{mA,W+B}(\alpha, \delta_F)$; $\mathrm{Re} = 2.5 \cdot 10^6$; $Ma = 0.6$

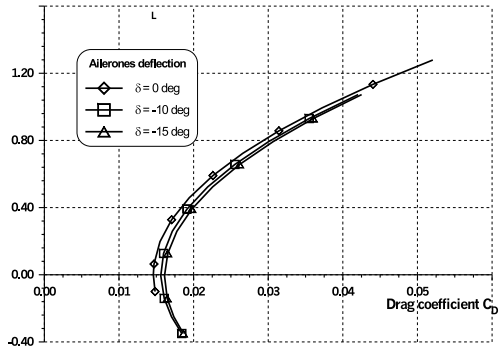

Fig. 30. HALE PW-114 – polar drag

Polar drag for the whole aircraft are given in Fig. 30. This drag consists of the parasite components (Tab. 7) depending on wetted area and the induced drag depending on the lift coefficient.

Table 7
C_{D0} breakdown

Parasite drag	C_D	S_i (reference area)	$C_{Di} * S_i/S$
Wing	0.0068	44.4	0.0068
Fuselage	0.005385	44.4	0.005385
Vertical stabilizer	0.008	3.83	0.0007
Nacelle	0.06	0.67	0.0009
Total parasite drag	0.0138	44.4	0.0138

An influence of the boundary layer on lift and pitching moment was shown in Figs. 31–32. It was found that in most of cases at small flight altitudes at small angles of attack the boundary layer influence can be neglected. However, it is not the case at high altitude (20 km, for example) and it is the reason why in all computational procedures when the aerodynamic characteristics were approximated, the boundary layer was included into the computational model.

Conditions of longitudinal equilibrium (trimming) were found for a number of altitudes, weights and flight scenario. As an example the lift and pitching moment coefficients versus angle of attack (weight of the aircraft

was changing, flight speed was constant) are presented in Figs. 33 and 34.

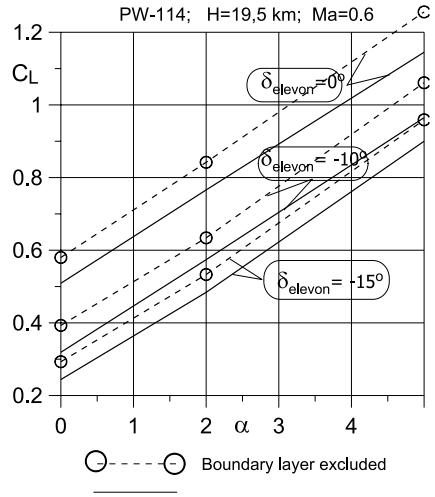

Fig. 31. Lift coefficients for clean wing and for extended elevons

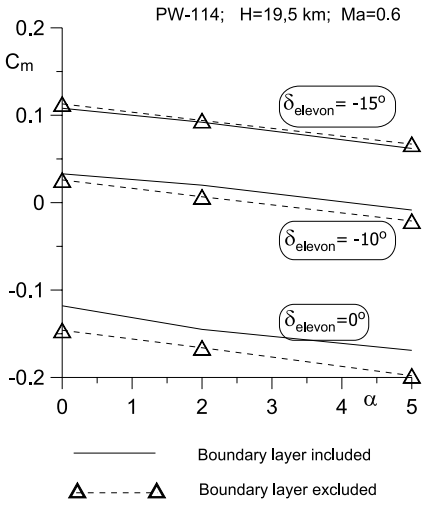

Fig. 32. Moment coefficients for clean wing and for extended elevons

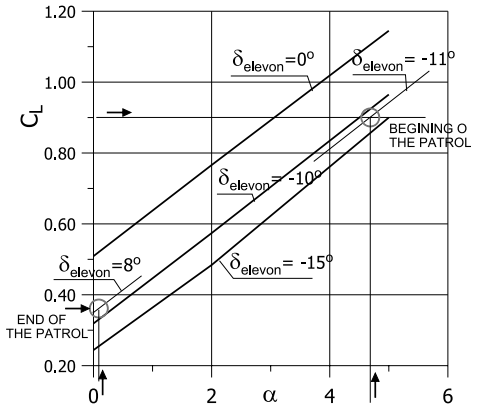

Fig. 33. PW114 – longitudinal trimming Lift versus angle of attack

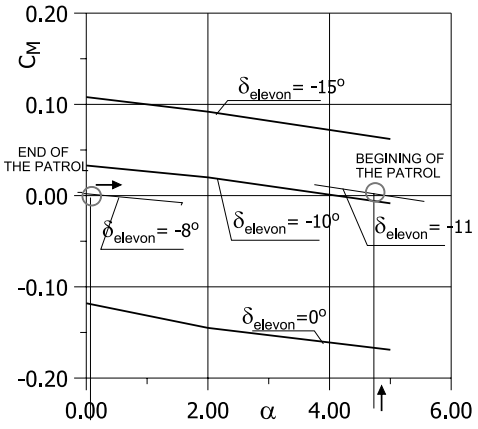

Fig. 34. PW114 – longitudinal trimming pitching moment versus angle of attack

5. Wing design

The wing consists of: torsion box, nose and movable parts: flap, spoilers, elevon and wingtip (Fig. 35). Double-circuit torsion box, made of epoxy-carbon composite takes the torsion loading (Fig. 36). Upper and lower skins are made of sandwich with filler made of polyurethane foam. The torsion box contains also: front spar, main spar and rear spar. Main spar flanges are made of carbon roving. Their sections were designed to use all fibres in the most efficient way. Spar walls are made of sandwich using carbon fabric and polyurethane foam. Control surfaces skins (both noses and rear skins) and internal walls are also designed as sandwich and are made of carbon fabrics.

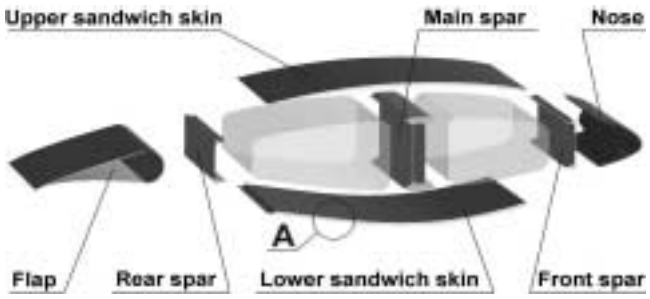

Fig. 35. Exploded view of the wing structure. Left wing is shown

5.1. Wing structure – an initial design. Initial design assumes application of two layers of fabric with specific weight of 163 g/m^2 (similar to the Interglas 98131) and two layers of fabric with specific weight of 93 g/m^2 (similar to the Interglas 98110) for the skins' structure. This would give the shear stress level of 20MPa in the most loaded region of the skin. Number of layers in the main spar wall will be variable along the span. There will be ten layers of the fabric with specific weight of 285 g/m^2 (similar to Interglas 98160) near the wing brackets.

Wing loading causes stress level of 52MPa in the D point of the manoeuvring envelope. Front and rear spar walls have structures made of three layers of the fabric with specific weight of 163 g/m^2. Shear modulus G=7GPa was assumed.

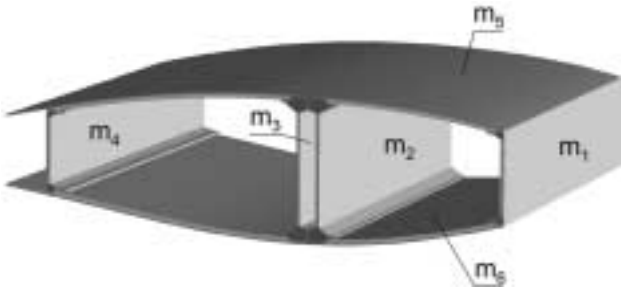

Fig. 36. Torsion box section

Table 8
Masses of the torsion box segment defined in Fig. 36

	Mass [kg]	%
m1	0.60	6.5
m2	3.17	34
m3	3.17	34
m4	0.59	6.5
m5	0.87	9.5
m6	0.88	9.5
Torsion box total	9.28	100

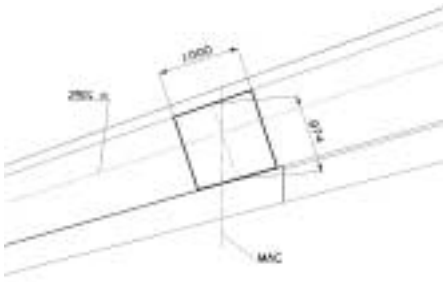

Fig. 37. Definition of the torsion box segment analysed in Tab. 8. Figure shows the top view of the left wing

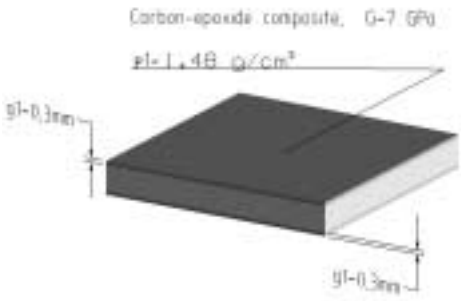

Fig. 38. Detail A from Fig. 35

Spar flanges were designed so that stress level is constant along the wing span. Initial design of control surfaces assumes application of two layers of carbon fabric with specific weight of 163 g/m^2 and one fabric layer with specific weight of 93 g/m^2. There will be three layers of the fabric with specific weight of 163 g/m^2 in the walls.

Weights of wing components are as follows: (1) torsion box with fuel ribs, nose and anti-icing installation (tube and diaphragm) – 96 kg; (2) control surfaces – 11.5 kg; (3) wingtip with brackets – 7.8 kg; (4) control surfaces' consoles – 3 kg; (5) actuators – 16.5 kg and; (6) fuel installation – 6 kg. The complete wing weight is equal to 140.8 kg. Total weight of both wings including various subsystems and installations is equal to 281.6 kg. Wing/fuselage bracket was ignored in the course of the wing weight and stiffness analysis. It is rigidly connected to the fuselage, so it was included in the fuselage weight.

5.2. Flutter analysis – the calculations method. Free vibrations of the structure were determined for flutter analysis. They were supplemented by rigid aircraft motion modes. Aerodynamic model and certain constants like air density, reference dimension or assumed Mach number were used for flutter analysis among free vibrations. Air density on the see level was assumed first. Then coefficient compliant with standard atmosphere was introduced for different altitudes.

Doublet Lattice Method (DLM, [28]) was applied to determine the nonstationary aerodynamic forces. DLM is a digital method based on double layer theory considering air compressibility. The method used to solve the flutter equation accepted airspeed as a parameter. This method provides better assessment of vibrations' damping for air speeds close to the critical flutter airspeed and possibility to determine vibration modes.

Assume that aircraft can be represented in terms of its normal modes of vibration [29]. For displacements $w(x, y, t)$ in the z direction normal to the plane of the planform, the normal mode shapes can be represented by $\phi(x, y)$ and the associated natural frequencies by ω_i. A typical displacement of the structure can be written as

$$w(x, y, t) = \sum_{i=0}^{n} \xi_i(t)\phi_i(x, y), \tag{11}$$

where $\xi(t)$ is the generalized coordinate of the i-th natural mode $\phi(x, y)$.

The so-called k-method or V-g-method was used to determine the stability boundary. In the V-g-method it was assumed that a generalized coordinate

$$\xi = qe^{i\omega t}, \tag{12}$$

where i is the imaginary unit, i.e. $i = \sqrt{-1}$.

The generalized equation of motion in the matrix, linearized form can be written as follows:

$$\left(-\omega^2 [M]_{15x15} + [K]_{15x15} + i [B]_{15x15}\right) \{q\}_{15x15} = -\rho\omega^2 [A(k)]_{15x15} \{q\}_{15x15}, \tag{13}$$

where:

$\{q\}$ — vector of generalized coordinates q_i of the i-th mode,

$[M]$ — mass matrix,

$[K]$ — stiffness matrix,

$[B]$ — damping matrix (damping is assumed to be proportional to displacement and in phase with displacement velocity),

ω — natural frequency,

i — imaginary unit,

$[A(k)]$ — aerodynamic matrix in complex form

$k = \omega b/V$ — Strouhal number

V — undisturbed flow speed,

b — characteristic length (assumed as half of root chord, i.e. $b = C_r/2$)

A number of figures has been placed below to show some details of a mathematical model employed to compute critical flutter speed.

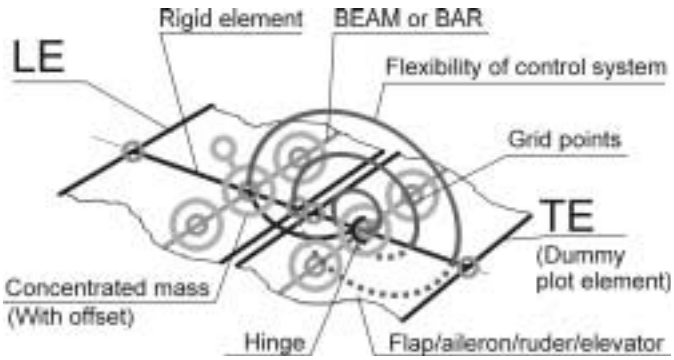

Fig. 39. Symbols used in modelling process

Elements used in the flutter modelling and shown in Fig. 37 are:

- NODAL POINTS (the so-called GRID) have 3 linear displacements and 3 angular displacements. NODAL POINTS are connected by BEAM and BAR elements (orange line segments at the figure).
- BEAM and BAR elements represent the structural stiffness.
- Masses are represented by big blue wheels and are allocated in the NODAL POINTS (i.e. in GRID).
- Actuator's stiffness' are represented by springs, shown at the figure as an amaranth zigzags. Small blue wheels represent the kinematic constraints.

Aerodynamic loads have been calculated basing on the oscillatory, subsonic lifting surface theory. A singular integral equation has the form

$$\frac{w(x,s)}{U_\infty} = \frac{1}{8\pi}\int\int_S \Delta C_p(\xi,\eta)K(x_0,y_0;\omega,M_\infty)\,d\xi\,d\eta, \quad (14)$$

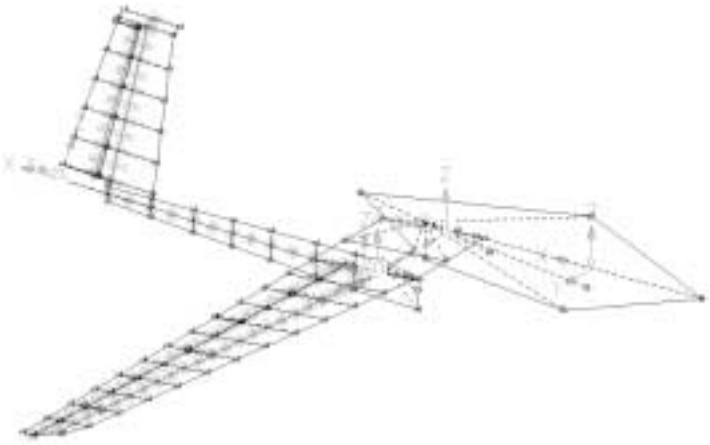

Fig. 40. Schematic representation of aircraft under flutter analysis, including global and local frame of reference. Nodal points (the so-called GRID) have 3 linear displacements and 3 angular displacement. Nodal points are connected by BEAM and BAR elements (at the figure marked as orange or red line segments, respectively). BEAM and bar elements represent the structural stiffness. Mass of the structure is represented by big blue wheels and is allocated in the nodal points (i.e. in GRID). Actuator's stiffness' are represented by springs, shown at the figure as a amaranth zigzags. Small blue wheels represent the kinematic constraints. This figure shows an arbitrary aircraft (not necessarily Blended Wing)

where (x, s) are orthogonal coordinates on the surface S such that the undisturbed stream is directed parallel to the x axis and

$$\Delta C_p = \frac{\Delta p}{\frac{1}{2}\rho_\infty U_\infty^2}, \quad (15)$$

is the dimensionless lifting pressure coefficient.

The kernel function for a nonplanar surface can be written as

$$K = -\exp\left(\frac{-i\omega x_0}{U_\infty}\right)\frac{K_1T_1 + K_2T_2}{r^2}, \quad (16)$$

where

$$r = \beta\sqrt{y_0^2 + z_0^2}, \quad (17)$$

$$x_0 = x - x,\ y_0 = y - h,\ z_0 = z - \zeta, \quad (18)$$

A set of linear equations in the form

$$\bar{w}_i = \sum_{j=1}^{n} D_{ij}\bar{p}_j, \quad (19)$$

where

$$D_{ij} = \frac{1}{8\pi}\Delta r_j \cos\lambda_j \int_{j_j} K[x_i, s_i); x_j(\mu), s_j(\mu)]d\mu, \quad (20)$$

enables us to find the dimensionless pressure coefficients if dimensionless normal velocities are known.

Aerodynamic model and certain constants like air density, reference dimension or assumed Mach number are used for flutter analysis based on free vibrations. Usually, air density at the see level is assumed first in the flutter analysis. Then coefficient compliant with standard atmosphere is introduces for different altitudes.

PK method was used to solve the flutter equation with air speed as a parameter. This method provides better assessment of vibrations' damping for air speeds close to the critical flutter airspeed and possibility to determine vibrations' modes. Assumption of one Mach number (despite obvious connection with airspeed that is a parameter in the PK method) allows for a substantial calculations' simplification in the course of initial analyses [29].

It was assumed that aircraft is symmetrical for purposes of calculations. This allowed to constrain the model to right part of the aircraft. Symmetrical and antisymmetrical vibrations were calculated separately.

The referred frequency k (*Strouhal number*) is usually based on the half of Mean Aerodynamic Chord (i.e. 0.5 of MAC $= 0.5 * 2.02 = 1.01$). Very often flutter is determined basing on 15 symmetric or antisymmetric free vibrations (including 6 modes of rigid aircraft motion).

Results of flatter analysis are usually presented on the plots $g(V)$ and $f(V)$, where g represents damping coefficient, that should be addend to receive constant amplitude vibrations, f – vibration frequency, V – equivalent airspeed (EAS). Positive value of g represents the danger of self-excited vibrations.

Internal damping is related to fictitious damping coefficient g. It is also known as a structural damping and can be considered in various ways. Presented calculations disregard structural damping in the phase of equation definition for flutter. Therefore, in the course of results analysis, it is reasonable to assume that divergent vibrations will appear for g values greater than internal structural damping. According to U.S. Department of Transportation, Federal Aviation Administration (FAA), *Advisory Circular No 23.629-1A* pp. 7 the internal structural damping "g" is equal to 0.02 or 0.03 considering the shape of $g(V)$ curve [30–31]. This assumption is represented by horizontal lines $g = 0.02$ and $g = 0.03$ on $g(V)$ plots. This method is simpler and provides a greater safety margin because real damping is usually greater than recommended in the Advisory Circular. Flutter vector is determined for selected points on $g(V)$ and $f(V)$ plots. This vector shows free vibrations' fractions in the flutter mode and phase shifts of all coordinates with respect to a selected coordinate in the mode under consideration.

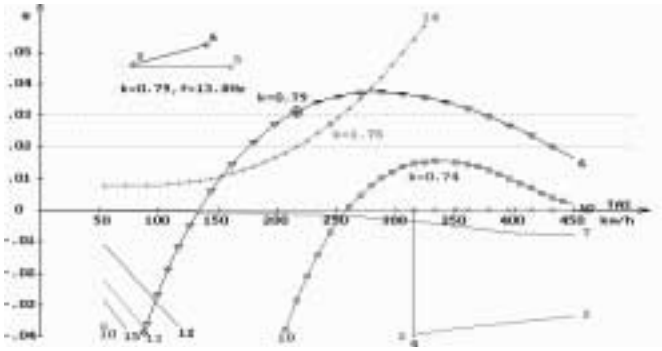

Fig. 41. Plot of g (structural damping coefficient) versus TAS. Mode number 6 at TAS=220 km/h leads to the flutter of symmetric fuselage bending coupled with symmetric elevator deflections (reduced frequency $k = \omega * C_r / V_\infty$)

5.3. Wing structure – an initial design. Flutter analysis has showed [32–34] that torsion box torsion rigidity is too small to achieve required critical flatter airspeed. That is why composite thickness will be increased in skins and walls of front and rear spar. The skins will contain two layers of the fabric with specific weight of 285 g/m^2 and two with specific weight of 163 g/m^2. Shear modulus G=16GPa was assumed.

Table 9
Masses of torsion box segment defined at Fig. 36

	Mass [kg]	%
m1	0.64	5
m2	3.17	27
m3	3.17	27
m4	0.63	5
m5	2.17	18
m6	2.17	18
Torsion box total	11.96	100

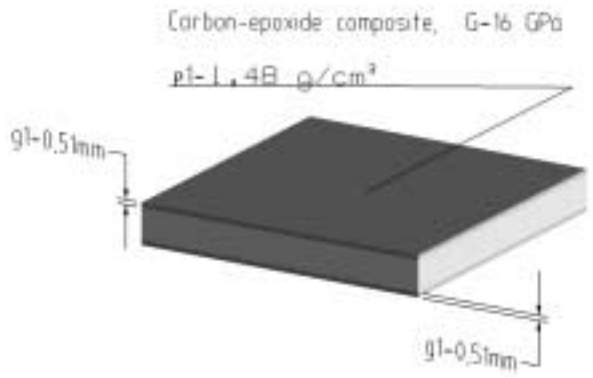

Fig. 42. Detail A from Fig. 35

An increase of skin thickness will also increases the wing bending rigidity slightly.

Weights of the wing components will be the following:
- torsion box with fuel ribs, nose and anti-icing installation (tube and diaphragm) – 196 kg
- remaining components listed in section 0
- additional glass fabric layer with specific weight of 105 g/m (similar to Interglas 91110) for skins faces – 3.6 kg
- lacquer – 6.9 kg

Left wing weight was increased to 170.3 kg, and the total weight of both wings became equal to 340.6 kg.

5.4. Stiffer wing compared to the initial version. Following the results of flutter analysis the wing torsion

box was essentially redesigned. Selected characteristic features of this redesign process are placed in the Tab. 10.

Table 10
Important design features and their values corresponding to wing redesign

Characteristic feature	formula	value
Thickness ratio of the composite in the skin structure	$(g_2/g_1) \times 100\%$	170%
Torsion rigidity ratio of torsion box	$(GJo_2/GJo_1) \times 100\%$	400%
Torsion angle ratio of a unit segment	$\varphi_2/\varphi_1 \times 100\%$	24.5%
Wing weight ratio	$(w_{w2}/w_{w1}) \times 100\%$	121%

Table 10 presents a very concise description of the redesign process of the wing to increase the critical flutter speed. Two layers of fabric with specific weight of 163 g/m^2 and the two next layers of specific weight of 93 g/m^2 were replaced by two layers of the fabric with specific weight of 285 g/m^2 and two with specific weight of 163 g/m^2. It resulted in the thickness ration increase on 170 % and the torsion rigidity ratio of the torsion box on 400%. More stiff torsion box will twist 24.5% that of initial design only and its total weight will be increased on 121%. The critical flutter speed was increased enough to be beyond the value of $1.2 \times V_D$, i.e. the so-called diving speed increased on 20%, required for certification process by typical Airworthiness Regulations.

In Table 11 there are critical flutter speeds computed at the see level, both for symmetric and antisymmetric models, under the assumption that the structural damping coefficient "g" is equal to 0.02. All stationary solutions (of zero frequency) are not included here.

6. Control system

Flight control system is used to both trim and control the aircraft in normal operation and to reconfigure the aircraft after a failure. All aerodynamic control surfaces are doubled or even three-folded to arrange redundancy, Fig.43. All these control surfaces are powered by electrical actuators 28VDC and governed by central flight control computer, also in redundant configuration. Because control surfaces have to be deflected dynamically (relatively fast), their actuators have also act quickly, without any excessive delay behind the electrical signal sent by on-board computer. Through the whole design effort it has been decided that the so-called COTS elements (Commercial Off The Shelve) will be used in all cases (if possible). The challenge in this case was to adjust the real hinge moment to the biggest one being possible to be transmitted by a actuator from the MOOG family, Fig. 44. MOOG's actuators are designed specially for Unmanned Arial Vehicles and for flight-by-wire systems. The lighter actuator will be, the lighter wing, lower its strain and stress level and as a result the more aerodynamically efficient aircraft.

Table 11
Critical flutter speed at the see level for selected computational variants

Specific model description	Aircraft weight [kg]	Symbol of symmetric model	Critical flutter speed V_{CR} [km/h]	Frequency [Hz]	Symbol of antisymmetric model	Critical flutter speed V_{CR} [km/h]	Frequency [Hz]
St	2307	50s	433	9.2	50a	479	12.4
$St + w$	2313	51s	503	8.8	51a	595	11.1
$St + f_2$	3375	52s	545	10.8	52a	565	9.2
$St + f_2 + w$	3381	53s	706	6.5	53a	622	8.5
$St + f_1 + f_2$	4635	54s	577	10.4	54a	442	10.7
$St + f_1 + f_2 + w$	4641	55s	702	6.3	55a	625	7.8
$St + f_1 + f_2 + f_3$	5004	56s	628	4.4	56a	664	5.6
$St + f_1 + f_2 + f_3 + w$	5010	57s	644	4.3	57a	674	5.3
$St + f_1 + f_2 + f_3 + f_B$	6224	58s	621	4.3	58a	664	5.6
$St + f_1 + f_2 + f_3 + f_B + w$	6230	59s	635	4.25	59a	674	5.34

where
St — Structure, on-board equipment and sensors only; no fuel
w — a balance wing tip weight (2×3.1344 kg)
f_B — fuel in the body (2×610 kg)
f_1 — fuel in the wing inner tanks (2×610.04 kg)
f_2 — fuel in the wing middle tanks (2×533.75 kg)
f_3 — fuel in the wing outer tanks (2×184.25 kg)

Even in a symmetric flight some of these control surfaces are deflected to trim the aircraft. For example, the high altitude loiter requires the elevons have to be deflected up on 11° (at the beginning of the mission) or at least 8° (at the end of the mission), see Figs. 33–34. Using the aerodynamic breakes, tab-flaps or elevons either to trim the aircraft or to overcome sudden gust the relatively high hinge moments could be produced when the pitching moment axes are located typically, i.e. symmetrically and not far from the local chord-line. These excessive pitching moments and corresponding large forces to be exerted by actuators can neither be essentially reduced by aerodynamic balance of a control surface nor by balance tab of Fletner type. It has been decided to overcome this design problem by shifting the hinge axis the resistant moment below the control chordline. Such a shifting results in an essential decreasing of the hinge moment coefficient, mainly due to the fact that now the aerodynamic drag exert a positive hinge moment about the hinge line, balancing the negative hinge moment exerted by aerodynamic lift of control surface, Fig. 45.

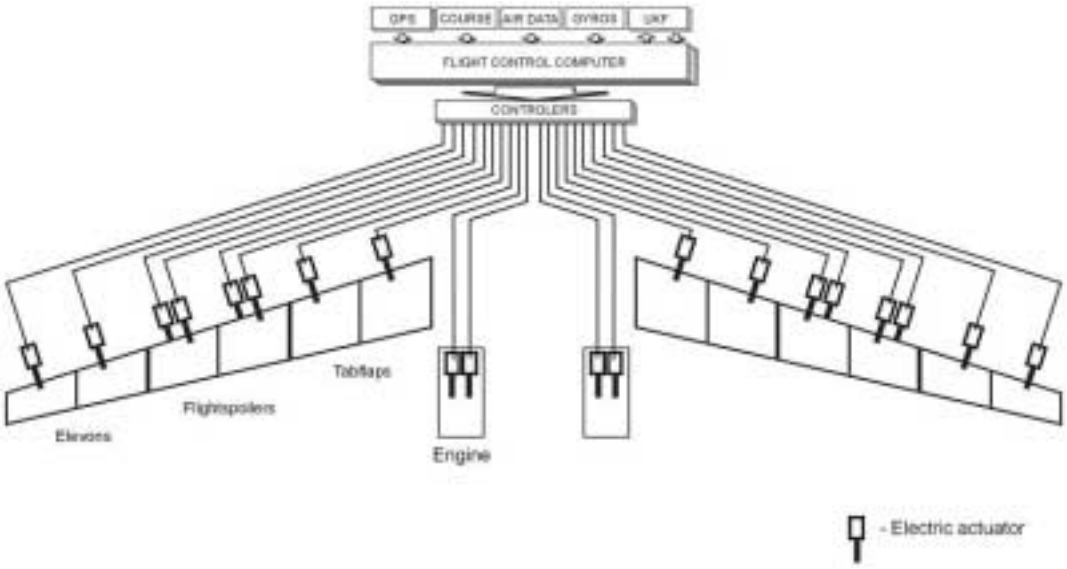

Fig. 43. HALE PW-114: the control system

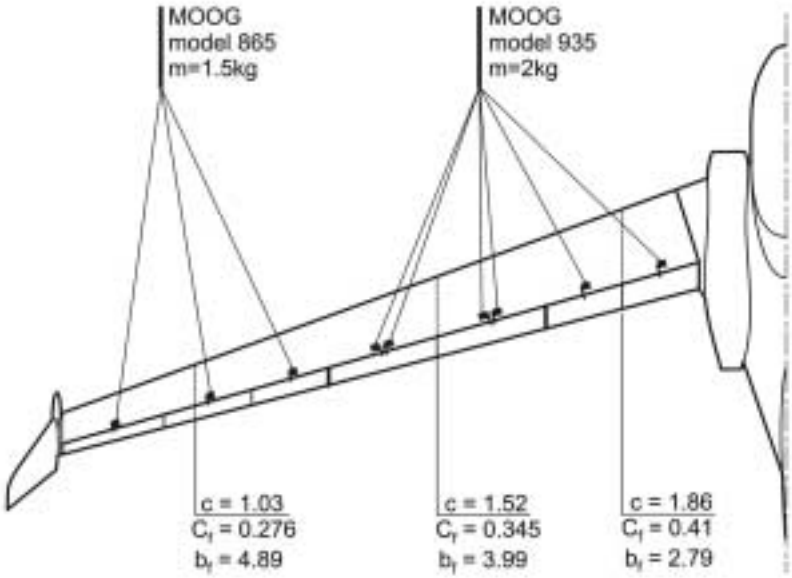

Fig. 44. Actuators situated along wing span

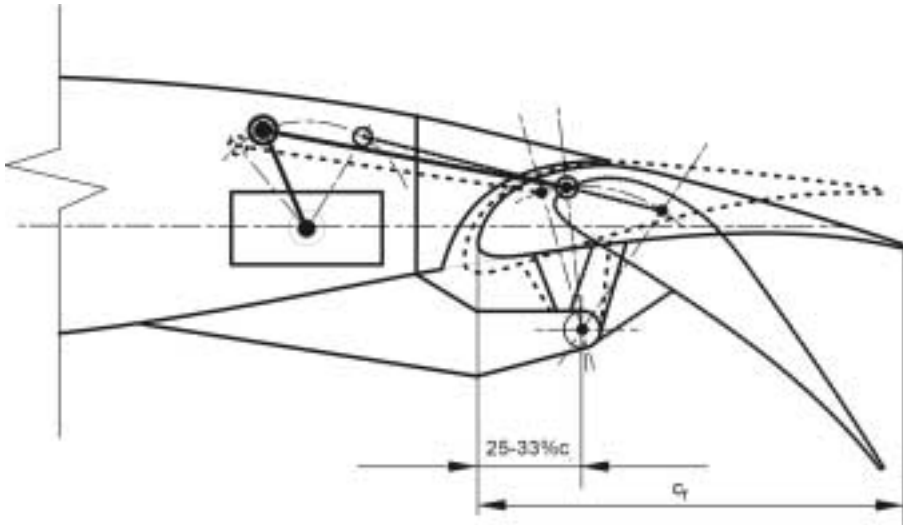

Fig. 45. Electrical actuator and its hinge axis – a schematic representation

7. Safety and reliability

Statistic data gathered for UAVs were used to conduct a reliability analysis [35]. Fig. 46 and Tab.12 show an example of the reliability analysis diagram. Both of them present standard series system with propulsion system, control system, communication system, ground station and others are singled out. The following equation can be used to determine Mean Time Between Critical Failures (MTBCF) for series system:

$$\frac{1}{MTBCF_S} = \sum_i \frac{1}{MTBCF_i}. \tag{21}$$

The reliability coefficient is equal to:

$$R_S(t) = \prod_i R_i(t), \tag{22}$$

where:

$$R_i(t) = \exp\left(-\frac{t}{MTBCF_i}\right). \tag{23}$$

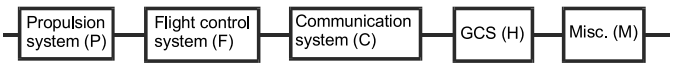

Fig. 46. Typical series system

The following equation can be used to determine MTBCF for parallel system:

$$MTBCF_S = MTBCF \cdot \left(1 + \frac{1}{2} + \frac{1}{3} + \ldots\right). \tag{24}$$

PW-114 has mixed series-parallel system (Fig. 47) with triple Flight Control system. Having MTBCF for separate subsystems one can compute the MTBCF for complete aircraft, see Tab. 13.

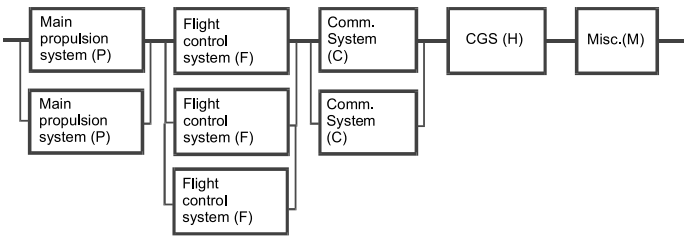

Fig. 47. Series-parallel PW-114 system

Other important characteristics, namely MTBL and MTBUCL are presented in Tab. 14. Critical Failures Probability $Q\ (t = 24)$ and Reliability $R\ (t = 24)$ in the 24 hrs missions, both for separate subsystems and for complete aircraft are given in Tab. 15.

Table 12
Reliability distribution for series UAV system

Distribution [%]	32	28	11	22	7
MTBCF [hrs]	MTBCFP	MTBCFF	MTBCFC	MTBCFH	MTBCFM
505	1600	1800	4500	2300	7000

Table 13
Reliability distribution for PW-114

Distribution [%]	32	28	11	22	7
MTBCF [hrs]	MTBCFP	MTBCFF	MTBCFC	MTBCFH	MTBCFM
692	2400	3300	6750	2300	7000

Table 14
Safety and Reliability parameters for UAVs

UAVs	MTBCF [hrs]	MTBL [hrs]	MTBUCL [hrs]
Any UAV (series system)	505	35 000	350 000
HALE PW-114	692	50 000	500 000

Table 15
UAV Critical Failures Probability $Q\ (t = 24)$ and Reliability $R\ (t = 24)$ (per 24 hrs mission)

	MTBCF [hrs]	Any UAV $R\ (t = 24)$	Any UAV $Q\ (t = 24) * 10^{-5}$	HALE PW-114 $Q\ (t = 24) * 10^{-5}$	HALE PW-114 $R\ (t = 24)$
Power Unit (P)	1600	0.9851	1480.0	22.1	0.9997
Flight Control (F)	1800	0.9867	1320.0	0.2	0.9999
Comm. (C)	4500	0.9946	530.0	2.8	0.9999
Human/GCS (H)	2300	0.9896	1040.0	1040.0	0.9896
Misc. (M)	7000	0.9965	342.0	342.0	0.9965
UAV System		0.9535	4712.0	1407.1	0.9859

8. Conclusion

This paper describes a design process of a HALE sensor-craft, developed for high altitude and long endurance surveillance missions. The main emphasis was put on aerodynamic and structural design to obtain an efficient, reliable and cost effective platform. Many modern software were used to make the design and optimisation process effective and fast. These software include UNIGRAPHICS, MSES, VSAERO, ANSYS, STB (a specialized software devoted to aerodynamic trim analysis, static and dynamic analysis and manoeuvrability) and other.

From the same beginning the design process was realized as an interdisciplinary approach, started from very precisely formulated requirements and all time the results were compared to performances of a reference aircraft (here it was Global Hawk build and flown by Northrop Grumman). The design process included a selection of thick laminar wing section, aerodynamic optimisation of swept wing, stability analysis, weight balance, structural and flutter analysis, many on-board redundant systems, reliability and maintability analysis, safety improvement, cost and performance optimisation. Presented paper focuses mainly on aerodynamic, wing design, longitudinal control and safety issues. A number of design iterations were performed to achieve the required aircraft performances and characteristics. This iteration number was relatively moderate (four only) due to employing a modern software and the essential role of theoretical analysis performed parallel to the design and redesign process. The so-called engineering intuition and experience is also important, however it can be overestimated, especially in a such demanding task as the HALE UAV design process is.

References

[1] Website: www.uavnet.com.

[2] D. Fulghum and R. Wall, "Israel's future includes armed, long-range UAVs", *Aviation Week and Space Technology*, 83–84 (2002).

[3] D. Fransaer and G. Lissens, "PEGASUS, the future of remote sensing", *UAVNET Meeting in Eilat*, Oct. 2002, www.uavnet.com.

[4] Sh. Tsach, "Advanced technologies for civil applications UAV's", *Rochester UAVNET Meeting*, July 2002, www.uavnet.com.

[5] A. Yaniv, "Review of IAI advanced design HALE UAV activities", *UAVNET Eilat Meeting*, Oct. 2002, www.uavnet.com.

[6] G. Goodman (Jr.), "Manned-unmanned synergy-US army UAV-related efforts gain momentum", *Armed Forces Journal International*, 56–61 (July 2002).

[7] D. Fulghum and R. Wall, "Israel pursues high tech despite war costs", *Aviation Week and Space Technology*, 78–80 (June 24, 2002).

[8] M. Allouche, "Civil UAV safety issues – airworthiness and operational certification aspects", *UAVNET, Stockholm*, Oct. 2001, www.uavnet.com.

[9] A. Morag, "UNITE UAV National Industry Team", *Eilat UAVNET Meeting*, Oct. 2002, www.uavnet.com.

[10] CAPECON Project No GRD1–2001–40162 (Civil UAV Applications and Economic Effectivity of Potential Configuration Solutions), Technical documents 2002–2004. V FR of European Union.

[11] A. Morag, "Aurora flight sciences corporate overview", *Eilat UAVNET Meeting*, Oct. 2002, www.uavnet.com.

[12] J. Vitali, S. Tsach and H. Avni, "Development Approach of the HERON Medium Altitude Long Endurance UAV", *20th ICAS Proc.*, Vol. I, 380–390 (Sept. 1996).

[13] Z. Goraj, Ph. Ransom and P. Wagstaff, "Dynamics and design aspects of future UAV's", *Aviation* VII (3), 20–36 (2003).

[14] Z. Goraj and A. Frydrychewicz, "Design challenges associated to development of a new generation UAV", *Proceedings of the First International Conference on Unmanned Arial Vehicles*, Kielce University of Technology, Kielce, 19 May 2004, 161–168 (2004), (in Polish).

[15] Z. Goraj, A. Frydrychewicz, C. de'Tallec and J. Hermetz, "HALE UAV platform optimised for a specialized 20-km altitude patrol mission", *Proc. of* 24$^{\text{th}}$ *ICAS Congress*, Yokohama 2004, Paper 1.6.3.

[16] Z. Goraj, Ph. Ransom and P. Wagstaff, "From specification and design layout to control law development for unmanned aerial vehicles – lessons learned from past experience", *Proceedings of V European Workshop on Aircraft Design Education*, Linköping, Sweden, 17–21 (June 2–4, 2002).

[17] Z. Goraj, A. Frydrychewicz and J. Winiecki, "Design concept of a high altitude long endurance unmanned aerial vehicle", *Aircraft Design – An International Journal* 2(1), 19–44.

[18] Z. Goraj, "Dynamics of a high altitude long endurance UAV", *ICAS Congress 2000*, England, Harrogate, paper 362, 10 (2000).

[19] Z. Goraj and T. Ueda, "Ultra light wing structure for high altitude long endurance UAV", *ICAS Congress 2000*, England, Harrogate, paper 476, 10 (2000).

[20] Z. Goraj, "Design and flight dynamics of a HALE UAV – HARVE-2", *Workshop for the Advancement of Unmanned Air Vehicles (UAVs) for Civilian Commercial Applications*, Paper no. 9, Israel Aircraft Industries, Israel, 15 (7–8 November 2000).

[21] Z. Goraj, "Civilian unmanned aerial vehicles – overview of European effort and challenges for the future", *Aviation Journal*, Vilnius 2003, *Aviation* VII(2), 1–18 (2003).

[22] Z. Goraj, "Dynamic characteristics of different UAV configurations", *UAVNET Capua Meeting*, Feb. 2002, www.uavnet.com.

[23] B. Holder, *Unmanned Air Vehicles – An Illustrated Study of UAVs*, Copyright @ 2001 by Bill Holder.

[24] *Jane's Unmanned Aerial Vehicles and Targets*, ed. Kenneth Munson, Couldson, Surrey CR5 2YH, UK 2001.

[25] www.airframe-technology.com/projects/global/index.

[26] www.airframe-technology.com/projects/predator/index.

[27] S. Tsach, A. Yaniv, H. Avni and D. Penn, "High altitude long endurance (HALE) UAV for Intelligence Missions", 20th *ICAS Proceedings*, I, 368–379 (Sept. 1996).

[28] W. P. Rodden and E. H. Johnson, *MSC/Nastran v.68. Aeroelastic Analysis*, Los Angeles, 1994.

[29] D. H. Hodges and G. A. Pierce, *Introduction to Structural Dynamics and Aeroelasticity*, Cambridge University Press, Cambridge, 2002.

[30] "Airframe and equipment engineering report", No. 45, *Simplified Flutter Prevention Criteria for Personal Type Aircraft*, Rev. 23889.

[31] "U.S. Department of transportation. Federal aviation administration", *Federal Aviation Regulations, Part 23, Amendments 1.42*.

[32] "U.S. Department of transportation. Federal aviation administration", *Advisory Circular* 23.629(1A), (1985).

[33] F. Kießling, *On Simplified Analytical Flutter Clearance Procedures for Light Aircraft*, DLR-Forschungsbericht, Göttingen 89–56 (1989).

[34] W. Stender and F. Kießling, *Aeroelastic Flutter Prevention in Gliders and Small Aircraft*, DLR-Mitteilung, Göttingen 91–03, (1991).

[35] Z. Goraj and S. Suchodolski, "Unmanned aerial vehicles of increased safety level", *Proc. of VI Conference on "Investigation Methods and Flight Tests of Aircraft"*, 161–168 (June 2004), (in Polish).